# Phase-shifting guided deep learning for single-frame fringe analysis: supplemental document

## 1. GENERAL PHASE RETRIEVAL FORMULA BASED ON LEAST-SQUARE ALGORITHM

Considering a general case of dual-frequency composite fringe, the captured patterns can be expressed as:

$$\begin{aligned} I_i &= A + B_H \cos(\varphi_H - \Delta_i) + B_L \cos(\varphi_L - \delta_i) \\ &= A + (B_H \cos\varphi_H)\cos\Delta_i + (B_H \sin\varphi_H)\sin\Delta_i + (B_L \cos\varphi_L)\cos\delta_i + (B_L \sin\varphi_L)\sin\delta_i \end{aligned} \tag{S1}$$

where $i = 1, 2, ..., N$, $A$ is the average intensity, $B_H$, $B_L$ are modulations corresponding to high- and low-frequency component, $\Delta_i$, $\delta_i$ are phase shifts corresponding to high- and low-frequency component. $\varphi_H$, $\varphi_L$ are phase value of the distorted fringe containing the depth information of the object surface. In matrix form, the $N$ equations expressed as Eq.(S1) can be rewritten as:

$$\begin{bmatrix} 1 & \cos\Delta_1 & \sin\Delta_1 & \cos\delta_1 & \sin\delta_1 \\ & & ... & & \\ & & ... & & \\ & & ... & & \\ 1 & \cos\Delta_N & \sin\Delta_N & \cos\delta_N & \sin\delta_N \end{bmatrix} \cdot \begin{bmatrix} A \\ B_H\cos\varphi_H \\ B_H\sin\varphi_H \\ B_L\cos\varphi_L \\ B_L\sin\varphi_L \end{bmatrix} = \begin{bmatrix} I_1 \\ I_2 \\ ... \\ ... \\ I_N \end{bmatrix} \tag{S2}$$

For short, the matrix equation can be written as: $\boldsymbol{A}\cdot\boldsymbol{\beta} = \boldsymbol{Y}$.

For a certain scene, $\boldsymbol{\beta}$ is the unknown parameters waiting to be figured out, $\boldsymbol{A}$ is independent variables with N-group different sampling values, $\boldsymbol{Y}$ is the dependent variables reflecting the parameters effect on independent variables. These linear equations satisfy the working conditions of least-square algorithm under FPP circumstances, so we choose LS algorithm to perform linear regression. According to LS algorithm in matrix form, we have:

$$\boldsymbol{\beta} = \left(\boldsymbol{A}^T\boldsymbol{A}\right)^{-1}\boldsymbol{A}^T\boldsymbol{Y} \tag{S3}$$

where

$$\boldsymbol{A}^T\boldsymbol{A} = \begin{bmatrix} N & \sum\cos\Delta_i & \sum\sin\Delta_i & \sum\cos\delta_i & \sum\sin\delta_i \\ \sum\cos\Delta_i & \sum\cos^2\Delta_i & \sum\cos\Delta_i\sin\Delta_i & \sum\cos\Delta_i\cos\delta_i & \sum\cos\Delta_i\sin\delta_i \\ \sum\sin\Delta_i & \sum\sin\Delta_i\cos\Delta_i & \sum\sin^2\Delta_i & \sum\sin\Delta_i\cos\delta_i & \sum\sin\Delta_i\sin\delta_i \\ \sum\cos\delta_i & \sum\cos\delta_i\cos\Delta_i & \sum\cos\delta_i\sin\Delta_i & \sum\cos^2\delta_i & \sum\cos\delta_i\sin\delta_i \\ \sum\sin\delta_i & \sum\sin\delta_i\cos\Delta_i & \sum\sin\delta_i\sin\Delta_i & \sum\sin\delta_i\cos\delta_i & \sum\sin^2\delta_i \end{bmatrix} \tag{S4}$$

$$\boldsymbol{A}^T\boldsymbol{Y} = \begin{bmatrix} \sum I_i \\ \sum I_i\cos\Delta_i \\ \sum I_i\sin\Delta_i \\ \sum I_i\cos\delta_i \\ \sum I_i\sin\delta_i \end{bmatrix} \tag{S5}$$

Ensure the invertibility of matrix $\boldsymbol{A}^T\boldsymbol{A}$, note $p_{i,j}$ as the element of column matrix $\boldsymbol{\beta}$, we obtain the general phase retrieval formula:

$$A = p_{1,1}\ ,\ \varphi_H = \tan^{-1}\frac{B_H\sin\varphi_H}{B_H\cos\varphi_H} = \tan^{-1}\frac{p_{3,1}}{p_{2,1}}\ ,\ \varphi_L = \tan^{-1}\frac{B_L\sin\varphi_L}{B_L\cos\varphi_L} = \tan^{-1}\frac{p_{5,1}}{p_{4,1}} \tag{S6}$$

Omitting the subscript, we define the numerator and denominator of arctangent function as $M$, $D$:

$$M = B\sin\varphi\ ,\ D = B\cos\varphi \tag{S7}$$

Therefore, we offer more detailed guidance for $B$ and $\varphi$ through 'Constraint1&2' in Section2.2.1.

It needs to be mentioned that, when standard phase-shifting encoding strategy is used for dual-frequency composite fringes, there needs to be some restrictions on the phase shifts. Considering

$$\begin{aligned}\Delta_i &= 2\pi(i-1)/N\\ \delta_i &= 2m\pi(i-1)/N\end{aligned} \tag{S8}$$

The calculation of $\boldsymbol{\beta}$ is simplified as:

$$\begin{bmatrix} A\\ B_H\cos\varphi_H\\ B_H\sin\varphi_H\\ B_L\cos\varphi_L\\ B_L\sin\varphi_L\end{bmatrix} = \boldsymbol{\beta} = \left(\boldsymbol{A}^T\boldsymbol{A}\right)^{-1}\boldsymbol{A}^T\boldsymbol{Y} = \begin{bmatrix} N & 0 & 0 & 0 & 0\\ 0 & N/2 & 0 & 0 & 0\\ 0 & 0 & N/2 & 0 & 0\\ 0 & 0 & 0 & N/2 & 0\\ 0 & 0 & 0 & 0 & N/2\end{bmatrix}^{-1}\begin{bmatrix}\sum I_i\\ \sum I_i\cos\Delta_i\\ \sum I_i\sin\Delta_i\\ \sum I_i\cos\delta_i\\ \sum I_i\sin\delta_i\end{bmatrix} \tag{S9}$$

Thus, we have

$$\begin{aligned}A &= \frac{1}{N}\sum I_i\\ \varphi_H &= \tan^{-1}\frac{B_H\sin\varphi_H}{B_H\cos\varphi_H} = \tan^{-1}\frac{\frac{2}{N}\sum I_i\sin\Delta_i}{\frac{2}{N}\sum I_i\cos\Delta_i}\\ \varphi_L &= \tan^{-1}\frac{B_L\sin\varphi_L}{B_L\cos\varphi_L} = \tan^{-1}\frac{\frac{2}{N}\sum I_i\sin\delta_i}{\frac{2}{N}\sum I_i\cos\delta_i}\end{aligned} \tag{S10}$$

Obviously, we need $\varphi_H \neq \varphi_L$. Besides, we need the arctangent function real-valued and not always be zero. Therefore, we have:

$$m \neq \begin{cases} kN\pm 1\\ kN/2\end{cases}\ k = 0,1,2... \tag{S11}$$

which is the same as in [1].

In this Section, we demonstrate that stPSC is just a special case with certain restrictions when phase shifts are equal-spaced over $2\pi$ period, and give the general formula for retrieving the wrapped phase of dual-frequency composite fringes.

## 2. OPTIMAL PHASE-SHIFTING RULES (OPSR)

### A. Theory

In Section 2.1, we briefly introduced the OPSR (large number, wide range, even distribution), which coincides with the intensity noise analysis for traditional fitting method. Since the rules as well as the training strategy can be used in single frequency fringe analysis (Section **Discussion and conclusion**), we take single frequency as an example to demonstrate the relationship between OPSR and noise-induced phase error.

Considering N-step single frequency fringes with phase shifts $\Delta_i$, the captured image can be expressed as:

$$I_i = A + B\cos\left(\Phi - \Delta_i\right) \tag{S12}$$

where $i = 1, 2, ..., N$, $A$ is the average intensity, $B$ is the modulation. Using the general phase retrieval formula in Section S1, we have:

$$\begin{bmatrix} A \\ B\cos\varphi \\ B\sin\varphi \end{bmatrix} = \boldsymbol{\beta} = \left(\boldsymbol{A}^T\boldsymbol{A}\right)^{-1}\boldsymbol{A}^T\boldsymbol{Y} = \begin{bmatrix} N & \sum\cos\Delta_i & \sum\sin\Delta_i \\ \sum\cos\Delta_i & \sum\cos^2\Delta_i & \sum\cos\Delta_i\sin\Delta_i \\ \sum\sin\Delta_i & \sum\sin\Delta_i\cos\Delta_i & \sum\sin^2\Delta_i \end{bmatrix}^{-1} \begin{bmatrix} \sum I_i \\ \sum I_i\cos\Delta_i \\ \sum I_i\sin\Delta_i \end{bmatrix} \tag{S13}$$

Ensure the invertibility of matrix $\boldsymbol{A}^T\boldsymbol{A}$, note $p_{i,j}$, $q_{i,j}$ as the element of column matrix $\boldsymbol{\beta}$ and matrix $\left(\boldsymbol{A}^T\boldsymbol{A}\right)^{-1}$ respectively, we obtain the phase retrieval formula:

$$\varphi = \tan^{-1}\frac{B\sin\varphi}{B\cos\varphi} = \tan^{-1}\frac{p_{3,1}}{p_{2,1}} = \tan^{-1}\frac{q_{3,1}\sum I_i + q_{3,2}\sum I_i\cos\Delta_i + q_{3,3}\sum I_i\sin\Delta_i}{q_{2,1}\sum I_i + q_{2,2}\sum I_i\cos\Delta_i + q_{2,3}\sum I_i\sin\Delta_i} \tag{S14}$$

Since $\Delta_i$ is pre-defined value, $\Delta_i$ and $q_{i,j}$ are both constant. Thus, the phase retrieval formula can be written as a quotient of linear combinations of $I_i$ :

$$\varphi = \tan^{-1}\frac{\sum_{i=1}^{N} a_i I_i}{\sum_{i=1}^{N} b_i I_i} \tag{S15}$$

where $a_i$, $b_i$ are real coefficients given by:

$$\begin{aligned} a_i &= q_{3,1} + q_{3,2}\cos\Delta_i + q_{3,3}\sin\Delta_i \\ b_i &= q_{2,1} + q_{2,2}\cos\Delta_i + q_{2,3}\sin\Delta_i \end{aligned} \tag{S16}$$

According to Ayubi's research [2], the noise-induced phase error can be defined as below:

$$\sigma_\phi^2 = \frac{\sigma_n^2}{2B^2}\sum_{i=1}^{N}\left(a_i^2 + b_i^2\right) \tag{S17}$$

where $\sigma_n$ is the standard deviation of the noise (assuming that the intensity noise is additive, white, Gaussian distributed variable), $\sigma_\phi$ is the standard deviation of phase error. For simplicity, we note:

$$c_n = \sum_{i=1}^{N}\left(a_i^2 + b_i^2\right) \tag{S18}$$

which is a noise coefficient decided by phase shifts. When $\Delta_i = 2\pi(i-1)/N$, we have $c_n = \frac{4}{N}$. So Eq.(S17) can be reduced to:

$$\sigma_\phi^2 = \frac{2\sigma_n^2}{NB^2} \tag{S19}$$

which is the same as the error in standard phase-shifting algorithm [3].

Therefore, Eq.(S17) represents the phase error for general phase-shifting algorithm with arbitrarily chosen $\Delta_i$ and the error is completely determined by $c_n$ under a fixed measurement environment and fringe modulation. For observing the relationship between phase shift and $c_n$, we first let $\Delta_i = \theta(i-1)/N$, which has a total phase-shifting range $\theta$ and the phase shifts are equal-spaced. Calculating the value of $c_n$ when $\theta$ changing from 0 to $2\pi$, $N$ changing from 3 to 15, we plot the graph in Fig.S1(a). For each $N$, the more close $\theta$ to $2\pi$, the lower $c_n$ is. For each $\theta$, the larger $N$ we choose, the lower $c_n$ is. These two observations verify the first two rules in OPSR (large sampling number and wide sampling range). When the phase shifts are not equal-spaced, there must be some of them closer to each other. These sampling points (close phase shifts) can be viewed as one equivalent point, thus actually brings a reduction in valid $N$. Hence, the third rule in OPSR (even sampling distribution) is proved.

To guide the selection of general phase shifts $\Delta_i$, we also give two quantified indicators to characterize OPSR: the equivalent phase-shifting steps $N_e$ and the equivalent phase-shifting coverage $C_e$. Fig.S2 shows the process of the algorithm to obtain $N_e$ and $C_e$. Since phase-shifting changes the periodic sinusoidal term to adjust the project pattern intensity, we first regulate all phase shifts into $[0, 2\pi)$ by mod operation. Then sort operation is applied to obtain a series of phase shifts $\psi_1, \psi_2, ..., \psi_N$ which is in ascending order. A slide window is used to detect the super close phase shifts and substitute them using a single equivalent value which is their mean value. The remaining phase shifts are expressed as $\psi_1', \psi_2', ..., \psi_{N_e}'$, and the number of

them is the equivalent phase-shifting steps $N_e$. Then we calculate the modified first difference of ${\psi_1}', {\psi_2}', ..., {\psi_{N_e}}'$:

$$\Delta {\psi_i}' = \begin{cases} {\psi_{i+1}}' - {\psi_i}' , i = 1, 2, ..., N_e - 1 \\ 2\pi + {\psi_1}' - {\psi_{N_e}}' , i = N_e \end{cases} \tag{S20}$$

The equivalent phase-shifting coverage $C_e$ can be defined as the variance of $\Delta {\psi_i}'$:

$$C_e = \sigma^2_{\Delta {\psi_i}'} \tag{S21}$$

When phase shifts are equal-spaced and have a total range of $2\pi$, $C_e$ equals 0. Uneven phase shifts distribution or phase-shifting range less than $2\pi$ will bring a rise in $C_e$. Therefore, we can use $N_e$ and $C_e$ to quantitatively judge the OPSR ($N_e$ the larger the better, $C_e$ the smaller the better). Applying this algorithm to $\Delta_i = \theta(i-1)/N$, which is discussed before and shown in Fig.S1(a), we choose $N = 12$ and plot the corresponding $C_e$ in Fig.S1(b).

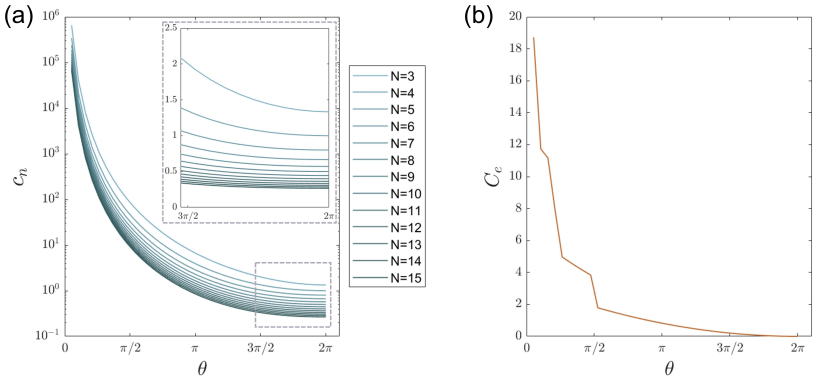


**Fig. S1.** Analysis for single frequency fringes with equal-spaced phase shifts. (a) Relationship between noise-induced error, phase-shifting steps and phase shifts. (b) Relationship between equivalent phase-shifting coverage and phase shifts.

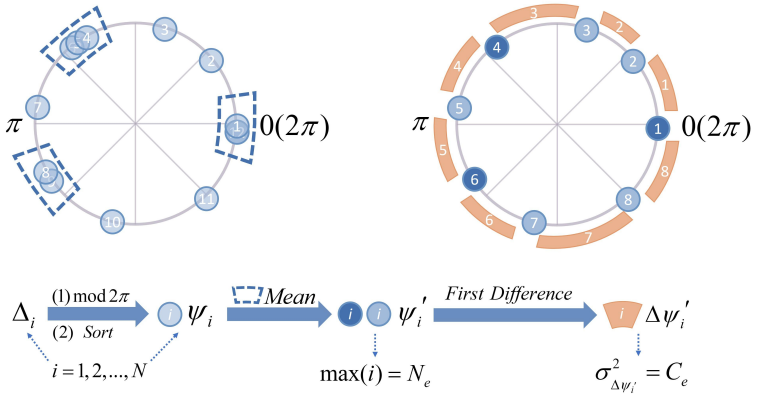


**Fig. S2.** Process for obtaining the equivalent phase-shifting steps and the equivalent phase-shifting coverage.

The analysis above qualitatively and quantitatively demonstrates that OPSR can roughly minimize the noise-induced phase error, which leads to a high-quality fitting result. Besides, $N_e$ and $C_e$ are crucial to create more non-repetitive and effective local intensity distribution, which influence the guiding effect to a great extent (see Section **Discussion and conclusion**). Thus, we union LS fitting algorithm and DL method into shared optimal phase-shifting rules.

### B. Application in fpPSC

Concerning the choice of PS-coefficient $k$ for fpPSC in training stage Step1, we combined noise-induced phase error and OPSR to make overall consideration.

Change the matrix in Eq.(S13) into dual-frequency form (Eq.(S4)-(S5)), referring to Eq.(S14)-(S18) we can calculate the $c_{n\_H}$ and $c_{n\_L}$ for high- and low-frequency wrapped phase. Then the $N_{e\_H}$, $C_{e\_H}$ and $N_{e\_L}$, $C_{e\_L}$ are calculated respectively. Setting a threshold as follows:

$$\begin{cases} \max(c_{n\_H}, c_{n\_L}) < 0.4 \\ \min(N_{e\_H}, N_{e\_L}) \geq 10 \\ \max(C_{e\_H}, C_{e\_L}) < 10^{-3} \end{cases} \tag{S22}$$

The only one PS-coefficient that satisfies the threshold is $k = 124$. Other typical $k$ are showed in Table S1, with corresponding phase shifts polar plot showed in Fig.S3.

**Table S1. Different PS-coefficient k and the corresponding evaluating indicators** (noise coefficient $c_n$, equivalent PS steps $N_e$, equivalent PS coverage $C_e$ of high- and low-frequency components).

| $k$ | $c_{n\_H}$ | $c_{n\_L}$ | $N_{e\_H}$ | $N_{e\_L}$ | $C_{e\_H}$ | $C_{e\_L}$ |
|---|---|---|---|---|---|---|
| 38 | 3.712 | 48.658 | 12 | 12 | $7.396 \times 10^{-32}$ | 1.295 |
| 76 | 0.347 | 0.432 | 6 | 12 | $5.325 \times 10^{-31}$ | 0.214 |
| 124 | 0.340 | 0.349 | 11 | 10 | $6.214 \times 10^{-4}$ | $2.998 \times 10^{-4}$ |
| 152 | 0.342 | 0.360 | 3 | 8 | $1.2282 \times 10^{-30}$ | $9.035 \times 10^{-5}$ |
| 204 | 0.351 | 0.338 | 12 | 6 | 0.049 | $5.325 \times 10^{-31}$ |

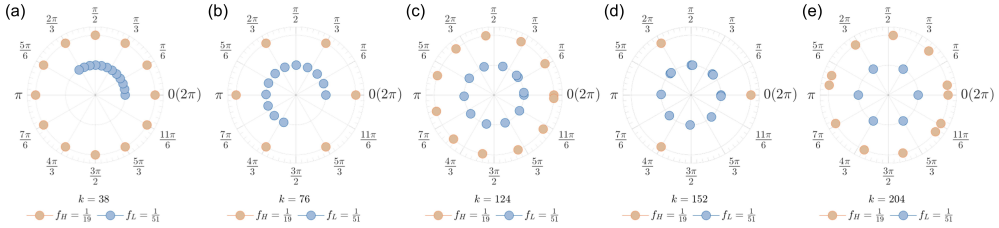


**Fig. S3.** Polar plot of phase shifts distribution with different $k$.

$k = 38$ makes high-frequency phase-shifting range equals $2\pi$ and achieves best $N_{e\_H}$ and $C_{e\_H}$. However, the noise-induced error is influenced by both high- and low-frequency due to the cross term of two frequency components in $c_{n\_H}$ and $c_{n\_L}$. Inefficient phase-shifting range of low-frequency component (Fig.S3(a)) leads to relatively high $c_{n\_H}$ and $c_{n\_L}$, which is also reflected in large $C_{e\_L}$. When the choice of $k$ makes phase shifts of both high- and low-frequency enjoy good equivalent coverage (low $C_{e\_H}$ and $C_{e\_L}$), like $k = 124$ and $k = 152$, the $c_{n\_H}$ and $c_{n\_L}$ indicating noise-induced error are relatively small. In this case, the quality of Loss0's label provided by LS algorithm using these $k$ is almost the same. Hence, we should choose the one that makes more effective $N_{e\_H}$ and $N_{e\_L}$.

To conclude, when phase shifts have a poor coverage of $2\pi$ range, OPSR and intensity error analysis coincide well. When phase shifts have a satisfying equivalent coverage, OPSR can give a choice more beneficial to the effect of physics loss (Loss1&2 in this work) in deep learning.

## 3. DNN RELATED SUPPLEMENTARY SPECIFICATIONS

### A. Loss functions construction

Taking high-frequency fringe phase retrieval as an example, we have the following 3 loss functions:

(1) In module 'Constraint0', for convenience, we directly using $y_{LS\_H}$ to constraint $y^0_{DL\_H}$, which is equivalent to Eq.(11) and Eq.(12). We first carry out LS algorithm to obtain numerator and denominator term of high-frequency component $y_{LS\_H} = (M_{LS\_H}, D_{LS\_H})$ using the input 12 fpPSC fringes (reasons for choosing '12 fpPSC' instead of Li's '12+12 PS', see Section S3.C), then construct the $Loss0$:

$$Loss0 = \frac{1}{H \times W} \sum_{h=1}^{H} \sum_{w=1}^{W} \left[ \left( y^0_{DL\_H} - y_{LS\_H} \right)^2 + \alpha_1 \cdot \left( \mathcal{F}(y^0_{DL\_H}) - \mathcal{F}(y_{LS\_H}) \right)^2 \right] \tag{S23}$$

where $\mathcal{F}(\cdot)$ means Fourier Transform, $\alpha$ is the hyperparameter. $Loss0$ can be viewed as Mean Square Error (MSE) in both spatial domain and fourier domain. In practice, adding fourier loss with proper $\alpha_1$ can bring more stable convergence and a bit accuracy improvement. Besides, to exclude shadow-noised regions that do not follow the relative relationship explained in Constraint1&2, we set a threshold for modulation $B_{LS\_H}$ to filter those invalid points. The filter mask $M$ can be expressed as:

$$M = \begin{cases} 1, \ B_{LS\_H} \geq Thr \\ 0, \ B_{LS\_H} < Thr \end{cases} \tag{S24}$$

In this work, $Thr$ is set to 0.02 (after data normalization).
(2) In module 'Constraint1', we construct $Loss1$ according to Eq.(8), also with both spatial and fourier term.

$$Loss1 = Loss1_{Spatial} + \lambda \cdot Loss1_{Fourier} \tag{S25}$$

$$Loss1_{Spatial} = \frac{\alpha_2}{N-1} \sum_{n=1}^{N-1} \frac{\sum_{h=1}^{H} \sum_{w=1}^{W} \left[ M \otimes \left( \sin(\varphi^0) - \sin(\varphi^n) \right) \right]^2 + \left[ M \otimes \left( \cos(\varphi^0) - \cos(\varphi^n) \right) \right]^2}{\sum_{h=1}^{H} \sum_{w=1}^{W} M} \tag{S26}$$

$$Loss1_{Fourier} = \frac{\alpha_1}{N-1} \cdot \sum_{n=1}^{N-1} \frac{\sum_{h=1}^{H} \sum_{w=1}^{W} \left[ \mathcal{F}\left( M \otimes \sin(\varphi^0) \right) - \mathcal{F}\left( M \otimes \sin(\varphi^n) \right) \right]^2 + \left[ \mathcal{F}\left( M \otimes \cos(\varphi^0) \right) - \mathcal{F}\left( M \otimes \cos(\varphi^n) \right) \right]^2}{H \times W} \tag{S27}$$

where $\varphi^n$ is the abbreviation of $\varphi^n_{DL\_H}$, and is the phase value of the first-step fringe calculated from the $n$-th group prediction (Eq.(7)), $M$ is the filter mask, $\otimes$ means the Hadamard product, $\alpha_1$, $\alpha_2$, $\lambda$ is the hyperparameter.
(3) In module 'Constraint2', we construct $Loss2$ according to Eq.(10):

$$Loss2 = \frac{1}{N-1} \sum_{n=1}^{N-1} \frac{\sum_{h=1}^{H} \sum_{w=1}^{W} \left[ M \otimes \left( B^0_{DL\_H} - B^n_{DL\_H} \right) \right]^2}{\sum_{h=1}^{H} \sum_{w=1}^{W} M} \tag{S28}$$

where $B^n_{DL\_H}$ is the modulation calculated from the $n$-th group prediction (Eq.(9)).

The overall loss can be expressed as:

$$Loss = Loss0 + \beta_1 \cdot Loss1 + \beta_2 \cdot Loss2 \tag{S29}$$

where hyperparameter $\alpha$, $\beta$, $\lambda$ is used to balance each losss order of magnitude, in order to achieve best guiding effect. In this work, $\alpha_1 = 1.11e^{-5}$, $\alpha_2 = 0.125$, $\lambda = 0.8$, $\beta_1 = 0.04$, $\beta_2 = 0.032$. The reason why $\alpha_1$ is comparatively small is that the magnitude of zero-frequency component in fourier spectrum is extremely large and is even larger after square operation.

### B. Unet architecture and network training

Fig.2(c) shows the architecture of Unet. The input tensor size is (B,1,H,W), where B is the batch-size (B=2 in this work), 1 represents the input channel of single frame composite fringe, H&W is the size of the input feature map. The input tensor is successively processed by a stack of convolutional blocks, pooling layers, upsampling blocks, and concatenate operations. In convolutional blocks, there is two convolutional layers (with kernel-3*3, stride-1 and zero-padding), and each activated by the rectified linear unit (ReLU). Besides, group normalization is inserted with group number equals a quarter of tensor channels, which stabilize the convergence compared with batch normalization especially when batchsize is small. Pooling layer is Maxpool2d with factor 2. In upsampling blocks, Upsample operation with scale factor 2 is followed by convolutional layers, group normalization and ReLU. Skip connection together with concatenation keeps feature map details well after pooling and upsampling. Lastly, a convolutional layer outputs a tensor with size (B,2,H,W), where 2 represents the output channel consisted of numerator and denominator feature map for arctangent function. The tensor size labeled at the side of the architecture figure shows the output feature map size of each convolutional block.

Before feeding the captured fringes with file format .bmp into network, we normalized them from [0,255] to [0,1] and converted them to .npy, then transformed them into four-channel tensor with size (B,1,H,W). Adam is chosen as the optimizer. To avoid overfitting, early stopping is adopted. It needs to be mentioned that the backward loss is the loss function (Eq.(S29)), but the loss value indicating early stopping is the spatial part of Loss0 (Eq.(S23)).

### C. Accuracy comparison between phase-shifting using dual-frequency composite fringes and single-frequency fringes

In training stage, when calculating $y_{LS}$ in Loss0 (Eq.(S23)), we choose 12 frequency-proportioned phase-shifting composite fringes ('12 fpPSC') with general phase retrieval formula (Section S1) instead of traditional 12 high-frequency fringes and 12 low-frequency fringes with standard phase-shifting algorithm ('12+12 PS'). Reasons are as follows.

Although traditional '12+12 PS' achieves higher accuracy, the measurement error of '12 fpPSC' is still on the same order of magnitude ($10^{-2}mm$) (Fig.S4 and Fig.S5). In Section **Experiment and results**, we demonstrate that PS-guided method using '12 fpPSC' in loss functions still performs far better than label-based method using '12+12 PS' to make GT. In other words, the proposed DNN using a bit worse label with strong prior knowledge constraints give a result closer to the better GT than the DNN directly using the better GT to guide the convergence. This experimental result enables researchers to just capture 12 fringes for each scene when making training dataset, instead of 36 fringes (12 high- and 12 low- and 12 dual-frequency fringes), which is less time and storage consuming in both data preparation and network training process.

To quantitatively evaluate the 3D reconstruction precision of '12+12 PS' and '12 fpPSC', we measured two standard ceramic spheres with radii $R = 25.4mm$. Fig.S4 and Fig.S5 show the precision analysis results of two methods, where Fig.S4(a) and Fig.S5(a) are the 3D reconstruction results, Fig.S4(b) and Fig.S5(b) respectively show the error distribution of the upper sphere, Fig.S4(c) and Fig.S5(c) show that of the lower sphere. Specifically, the ground-truth values of both of them are generated by fitting spheres using 3D reconstruction data. For the upper sphere, the root mean square (RMS) error of two methods are 0.053 mm and 0.068 mm, respectively. For the lower sphere, RMS of two methods are 0.042 mm and 0.056 mm, respectively. '12 fpPSC' achieves comparable precision in both spheres' measurement. Therefore, the proposed '12 fpPSC' is capable of obtaining $y_{LS}$ in training stage.

## REFERENCES


1. W. Guo, Z. Wu, Y. Li, *et al.*, "Real-time 3D shape measurement with dual-frequency composite grating and motion-induced error reduction," Opt. Express **28**, 26882 (2020).
2. G. A. Ayubi, C. D. Perciante, J. M. Di Martino, *et al.*, "Generalized phase-shifting algorithms: Error analysis and minimization of noise propagation," Appl. Opt. **55**, 1461 (2016).
3. C. Zuo, S. Feng, L. Huang, *et al.*, "Phase shifting algorithms for fringe projection profilometry: A review," Opt. Lasers Eng. **109**, 23–59 (2018).

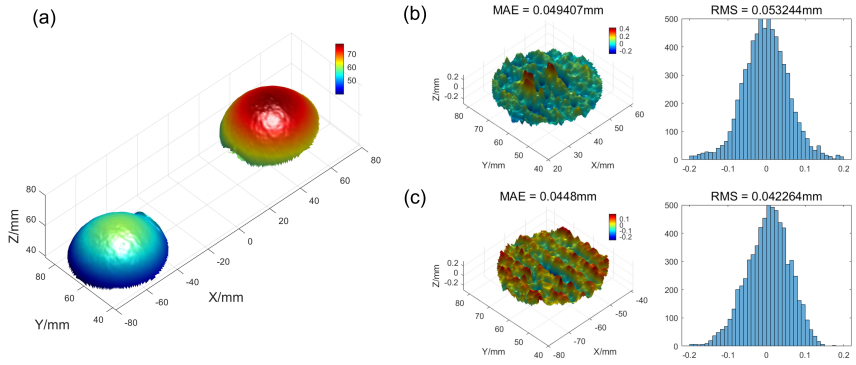


**Fig. S4.** Precision analysis of '12+12 PS' using two standard ceramic spheres. (a) 3D reconstruction results. (b, c) Error map and error distribution.

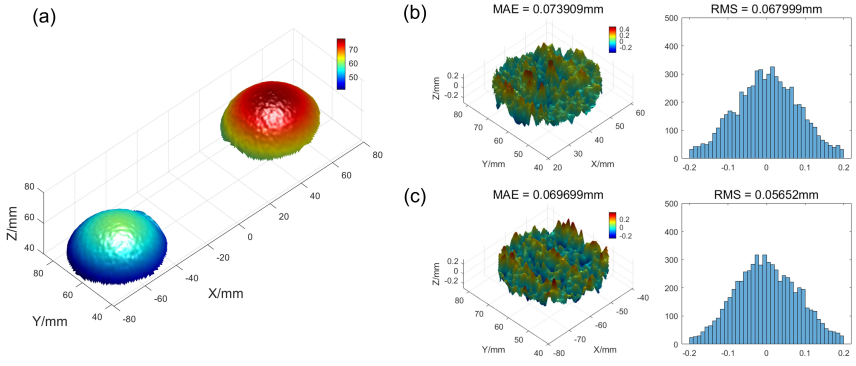


**Fig. S5.** Precision analysis of '12 fpPSC' using two standard ceramic spheres. (a) 3D reconstruction results. (b, c) Error map and error distribution.